Fluorescence quenching in hybrid solar cells based on electrodeposited ZnO

V. FIGÀ[*,a], H. DERBAL HABAK[b], B. KULYK[c], M. ABBATE[a]
[a]*Department of Physics and Chemistry, University of Palermo, Viale delle Scienze, Bd.17 – 90128 Palermo, Italy*
[b]*Laboratoire de Physique des Interfaces et des Couches Minces (LPICM) UMR7647, Ecole Polytechnique, Route de Saclay - 91128 Palaiseau Cedex France*
[c]*Chair of Solid State Physics, Department of Physics, Ivan Franko National University of Lviv, Dragomanova Street, 50, UA-79005 Lviv, Ukraine*

A study about fluorescence phenomena in hybrid donor-acceptor interfaces based on electrodeposited zinc oxide (e-ZnO) having different architectures is performed. In particular ITO/ZnO/P3HT and ITO/ZnO/P3HT:PCBM are investigated and their photoluminescence responses are compared with those of ITO/P3HT and ITO/P3HT:PCBM. As expected, ITO/ZnO/P3HT:PCBM and ITO/P3HT:PCBM present higher exciton quenching than ITO/ZnO/P3HT and ITO/P3HT respectively. Furthermore, the hybrid configuration ITO/ZnO/P3HT:PCBM displays a higher quenching percentage in a wider wavelength range than ITO/P3HT:PCBM, indicating a better photo-induced charge separation in e-ZnO based hybrid devices.

(Received October 29, 2012; accepted September 18, 2013)

Keywords: Hybrid solar cells, Zinc oxide, Poly 3-hexylthiophene, [6,6]- phenyl C60 butyric acid methyl ester

1. Introduction

Hybrid solar cells are optoelectronic devices for solar energy conversion into electricity made of both organic and inorganic materials. Generally, in these devices, conjugated polymers behave like electron donors and inorganic semiconductors like electron acceptors [1].

The aim of fabricating hybrid solar cells is to exploit the advantages of both conjugated polymers and inorganic semiconductors in order to increase conversion efficiencies. Organic materials are cheap, easy to process, lightweight and have high absorption coefficients; inorganic semiconductors have good mechanical and electronic properties such as high charge carriers mobility.

Among organic materials, poly 3-hexylthiophene (P3HT) and poly 3-hexylthiophene:6,6-phenyl C60 butyric acid methyl ester (P3HT:PCBM) blends have been widely investigated. P3HT is an electron donor with a band gap of 1.9 eV [2] and a very high hole mobility [3]. It is considered a promising material for photovoltaics [4-6]. PCBM is an electron acceptor that added to P3HT in the form of P3HT:PCBM blend allows a better exciton quenching and a higher power conversion efficiency.

At the present, organic BHJ solar cells have reached a conversion efficiency of 8.13% [7]

Among inorganic materials, ZnO has received interest due to its optical and electronic properties but also for its high mechanical and chemical stabilities.

It is a wide band gap oxide semiconductor that can be prepared as thin film by different methods such as pulsed laser deposition [8], radio frequency magnetron sputtering [9], sol gel processing [10], vapour deposition [11], molecular beam epitaxy [12], metal organic chemical vapour deposition (MOCVD) [13], electron beam evaporation [14], spray pyrolysis [15], chemical and electrochemical deposition [16,17]. The latter displays several advantages because allows a very good control of thickness and morphology; furthermore, experiments are rapid and cheap.

Electrochemical preparation of ZnO is performed in a common three electrodes cell using a suitable precursor as electrolyte; different conductive substrates - such as gold, graphite, ITO, etc. - can be used as working electrodes.

Electrochemical methods allow to obtain very good polycrystalline ZnO films at relative low temperatures - around 75°C - and more recently at room temperature reducing the processing costs [18].

ZnO thin films are transparent in the visible region of the spectrum and their direct energy gap - between 3.2 eV and 3.4 eV at room temperature - is located in the UV region.

n-type semiconducting ZnO has been already used in hybrid solar cells together with P3HT:PCBM blend [19] and together with P3HT as bulk heterojunction [20]. But at the present, the conversion efficiency of ZnO based hybrid devices is still around 2.5% [19].

In comparison with organic solar cells, hybrid ones have lower conversion efficiencies due not only to hybrid interfaces but also to: the contact area between donors and acceptors, processing conditions, roughness factor, thickness, etc. which influence their optical and electrical properties.

The study and the optimization of the different interfaces play a fundamental role for enhancing the performances of a hybrid PV device.

In this work hybrid solar cells with different architectures based on electrodeposited ZnO are fabricated and their photoluminescence responses are studied. The investigated devices are: a bi-layer heterojunction solar cell - ITO/ZnO/P3HT - and a device which is similar to both bi-layer and bulk heterojunction solar cells – ITO/ZnO/P3HT:PCBM.

The two devices are schematically displayed in Fig. 1.

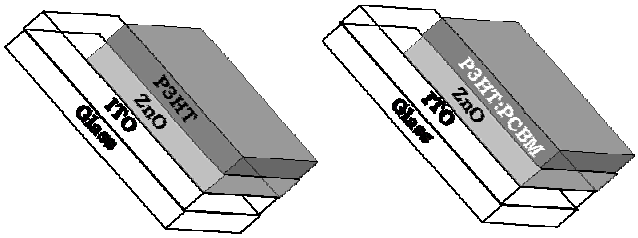

Fig. 1. Schematic representation of ZnO based hybrid solar cells.

The contact between ITO and ZnO has been obtained by electrochemical deposition of ZnO from a solution containing a suitable precursor; the contacts ZnO/P3HT and ZnO/P3HT:PCBM have been obtained by the spin coating of the polymers on the previously electrodeposited ZnO.

2. Experimental

ZnO thin films have been produced by means of electrochemical deposition on ITO coated glasses ($R \leq 7\ \Omega cm^{-2}$; thickness = 1.1 mm, Praezisions Glas & Optik GmbH), using a three electrodes cell as electrochemical reactor. The working electrode is ITO coated glass, the counter and the reference electrodes are graphite and saturated calomel electrode (SCE – with a potential of +0.25 V/NHE) respectively. The electrolytic solution is an aqueous solution of 0.1 M $Zn(NO_3)_2 \cdot 6H_2O$ (≥98% Sigma-Aldrich). Before experiments, ITO coated glasses have been cleaned in distilled water and RBS detergent for 30 minutes in ultrasonic bath and rinsed in acetone (CHROMASOLV, for HPLC, ≥99.9% Sigma-Aldrich). The electrodeposition of ZnO thin films is performed by applying a constant potential (potentiostatic method) between the working and the reference electrodes by means of a Potentiostat / Galvanostat (EG&G mod. 273A) connected to the cell.

P3HT (90-93% regioregularity, Rieke Metals) and PCBM (>99.9% SES Research) have been dissolved in chlorobenzene (99% anhydrous, Sigma-Aldrich) and deposited both on ITO and ZnO using a spin coater.

The experimental thickness has been estimated using a Profilometer (Dektak 8, Veeco).

The optical characterization consists in recording both absorbance and fluorescence spectra by means of a Perkin-Elmer Lambda 900 spectrophotometer and a fluorescence-spectrophotometer Hitachi F-4500, respectively. Absorption spectra are recorded for characterizing ZnO, P3HT and P3HT:PCBM; fluorescence spectra are recorded for characterizing ZnO, P3HT, P3HT:PCBM, ZnO/P3HT and ZnO/P3HT:PCBM.

3. Results and discussion

3.1 Electrochemical deposition and optical characterization of ZnO films

ZnO films have been electrodeposited by applying a constant potential of -1.0 V vs. SCE and the current density versus time plot has been recorded. According Izaki et al. [21] the reactions taking place at the working electrode are:

$$NO_3^- + H_2O + 2e^- \rightarrow NO_2^- + 2OH^- \quad (1)$$

$$Zn^{2+} + 2OH^- \rightarrow Zn(OH)_2 \quad (2)$$

Equation (1) represents the cathodic generation of hydroxyl ions followed by the chemical formation of hydroxide (2).

In order to obtain zinc oxide, the temperature of the cell has been thermo-stated at 75°C. In these conditions the de-hydration of zinc hydroxide and the precipitation of zinc oxide on working electrode take place according to the following reaction (3):

$$Zn(OH)_2 \rightarrow ZnO\downarrow + H_2O \quad (3)$$

Fig. 2 displays the current versus time characteristic recorded during zinc oxide electrodeposition at U_E= -1.0 V/SCE.

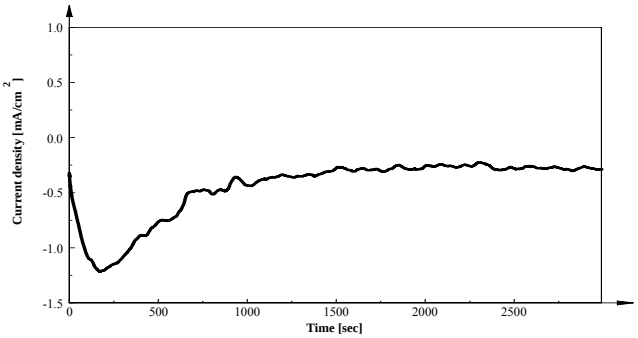

Fig. 2. Current density versus time recorded during ZnO electrodeposition on ITO in 0.1 M $Zn(NO_3)_2$. Applied potential U_E= -1.0 V/SCE.

Current density versus time plot displays a cathodic current peak at -1.2 $mAcm^{-2}$ and 185 s, which can be attributed to the processes of nucleation and growth before

the working electrode is completely covered with ZnO. After that, current density reaches a steady state value of -0.3 $mAcm^{-2}$ which can be associated to the increasing in film thickness. This value suggests that ZnO thin films deposited in the mentioned experimental conditions are good conductors.

It is known from Faraday law that the charge circulated during the electrodeposition corresponds to the value of the film theoretical thickness. Circulated charge is calculated by integrating current versus time plot in the time domain and its value is 1.33 C cm^{-2}.

The real thickness of ZnO films is estimated using a profilometer. According to these measurements, thickness shifts between 0.5 and 0.8 μm. On considering the circulated charge value, a faradic efficiency between 50% and 80% is evaluated.

Optical characterization of ZnO films is performed by recording absorption spectra in the UV, VIS, and NIR regions, from 200 nm to 900 nm. On comparing absorption spectra of ZnO films with different thicknesses, the same shape is found but higher absorbance values in the case of thicker films; these results are in agreement with the Lambert-Beer-Bouguer law. All the absorption spectra display maximum values at 338 nm and 361 nm for thinner (0.5 μm) and thicker (0.8 μm) films, respectively, so the wavelength corresponding to the absorption peak increases with the increasing in film thickness. The dependence of the absorption edge location on the thickness of ZnO films suggests also the dependence of the optical band gap value on the charge circulated during the electrodeposition process [22].

For direct semiconductors such as ZnO, the optical band gap (E_g) can be obtained by plotting $(\alpha h\nu)^2$ *vs* hν - where α is the absorption coefficient and hν is the incident radiation energy - and extrapolating the straight line portion of this plot to the radiation energy axis.

ZnO absorption coefficient is calculated from the absorbance spectra corrected for the ITO absorbance, using the following equation:

$$\alpha = \frac{OpticalDensity \times Ln10}{thickness[cm]} \tag{4}$$

Fig. 3 shows the optical density spectra of 0.5μm thick ZnO film and the best fitting of the $(\alpha h\nu)^2$ vs. hν plot.

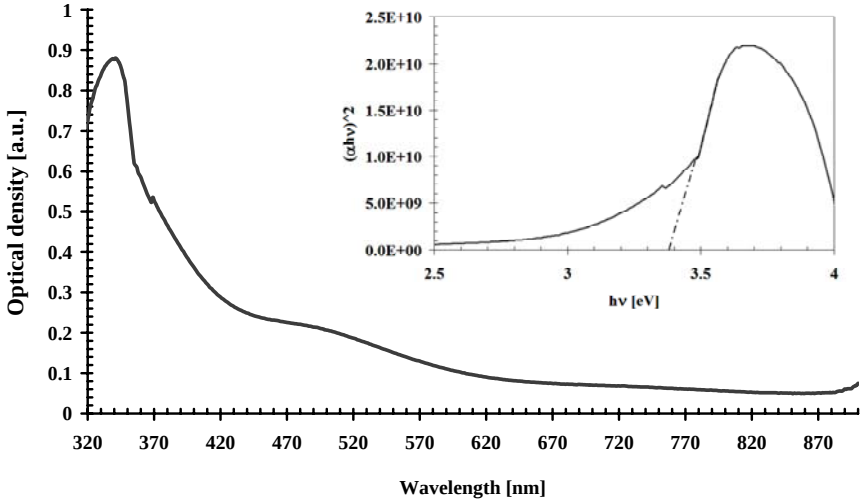

Fig. 3. Optical density spectra of 0.5 μm-thick ZnO film. Inset: Best fitting of the $(\alpha h\nu)^2$ vs. hν plot.

From the x- axis intercept, an optical band gap of 3.38 eV is found. This value is in agreement with literature data [23,24].

3.2 Preparation and optical characterization of the active layers

P3HT and P3HT:PCBM thin films have been prepared using the spin coating technique. This technique consists in the deposition of a liquid phase to the substrate surface and in the rotation of the substrate with fixed or changing angular velocity. The rotational movement of the substrate causes its complete coverage by a thin film. The thin film thickness depends on different parameters such as the angular velocity, the viscosity of the liquid phase and the substrate [25].

P3HT and P3HT:PCBM (1:0.8) are dissolved in chlorobenzene, stirred all night long and spin coated on ITO in two steps with different angular velocity, acceleration and duration. Thicknesses less than 1μm have been obtained.

Optical characterization of P3HT and P3HT:PCBM thin films has been performed by recording absorption spectra in the UV, VIS, and NIR regions, from 300 nm to 800 nm after thermal annealing at 100 °C for 10 minutes. Thermal treatment is necessary for enhancing P3HT and P3HT:PCBM crystallization and domains separation and consequently for extending absorption in the long

wavelengths region allowing an increasing of solar cells current density [26].

Fig. 4 displays absorbance versus wavelength plots of P3HT and P3HT:PCBM. P3HT absorbs in the wavelength range between 350 and 660 nm and presents a maximum of absorption at around 525 nm. P3HT:PCBM absorbs between 300 and 660 nm and displays a maximum of absorption at around 511 nm. Both P3HT and P3HT:PCBM are transparent for wavelengths above 660 nm.

It is known that P3HT behaves as a p-type semiconductor. According to the exciton model, the optical transition corresponding to the absorption peak of conjugated polymers such as P3HT is due to the promotion of an electron from the ground state (π) to an upper electronically excited state (π^*) which takes the configuration of a quasi-particle and can be considered as an electron/hole pair. By plotting $(\alpha h\nu)^2$ *vs* $h\nu$ and extrapolating the straight line portion of the plot to the x-axis, an optical band gap of 1.9 eV is estimated in agreement with literature data [27,28].

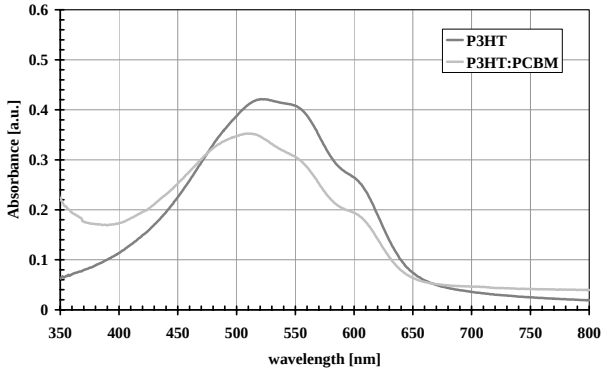

Fig. 4. Absorption spectra of ITO/P3HT and ITO/P3HT:PCBM films.

3.3 Steady state fluorescence studies

Fluorescence is a radiative emission phenomenon occurring from a body when it interacts with an electromagnetic radiation of suitable wavelength. Fluorescence studies give information about the efficiency of a photovoltaic device; in fact, photoluminescence (PL) quenching is a consequence of an efficient photo-induced charge transfer across different layers of a solar cell.

Fluorescence spectra have been recorded by applying excitations of different wavelengths perpendicularly to the samples surface. Fluorescence spectra of ZnO electrodeposited on ITO, P3HT and P3HT:PCBM spin coated on ITO have been compared with fluorescence spectra of ZnO/P3HT and ZnO/P3HT:PCBM at the same excitation wavelengths. Fig. 5 shows P3HT and P3HT:PCBM fluorescence spectra recorded at the excitation wavelength of 530 nm. P3HT and P3HT:PCBM emit radiatively from 600 to 800 nm. Both P3HT and P3HT:PCBM blend display two emission peaks at 660 and 720 nm respectively. These emission phenomena occur at lower energies than absorption. This result suggests a different conformation between the ground and the excited states.

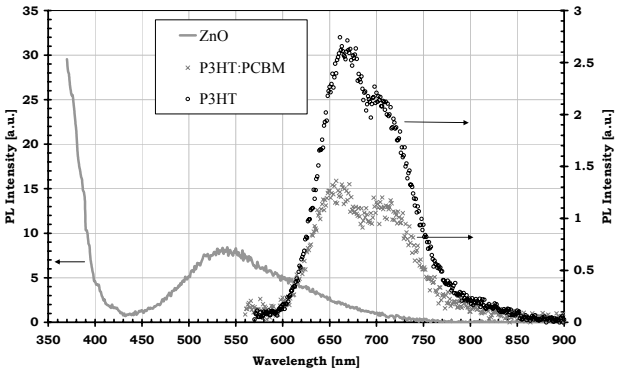

Fig. 5. ITO/P3HT and ITO/P3HT:PCBM fluorescence spectra recorded at the excitation wavelength of 530 nm. Fluorescence spectra of ITO/ZnO film. Excitation wavelength: 350 nm.

Photoluminescence emission intensity is lower in the case of P3HT:PCBM blend and it suggests a more efficient excitons quenching than in P3HT. By comparing PL spectra of P3HT and P3HT:PCBM, it is possible to estimate the quenching percentage; this is calculated as the difference between P3HT and P3HT:PCBM fluorescence intensities divided by P3HT fluorescence intensity. The maximum value of quenching percentage is 60% at 1.82 eV emission.

Fluorescence spectra from 370 to 900 nm have been recorded by irradiating ZnO films with a light beam having a wavelength of 350 nm (see Fig. 5).

Fluorescence versus wavelength plot displays two peaks; one is located in the ultraviolet region and the other in the visible region. The first peak is not well evidenced because of the initial value of the wavelength scan but we can consider that it is located at around 360 nm [29]. The correspondence between fluorescence and absorbance peaks in the UV region suggests that, in this region, the emission is caused by excitons deactivation.

The second emission peak corresponds to 540 nm. The location in the visible region suggests emission phenomena at lower energies caused by the presence of intrinsic or extrinsic defects, such as zinc vacancies, oxygen vacancies, interstitial zinc and interstitial oxygen.

From fluorescence spectra it is possible to obtain information about the quality of the films. On considering the high ratio between the maximum photoluminescence intensity in the ultraviolet region and in the visible region, we can conclude that ZnO films obtained by means of electrodeposition technique in the above mentioned experimental conditions, present a very high quality. Furthermore, from photoluminescence spectra we can confirm that the films electrodeposited in the above mentioned experimental conditions are not zinc hydroxide but zinc oxide. In fact, from literature it is known that zinc hydroxide behaves like a transparent layer that does not display its own photoluminescence spectrum [30].

Fig. 6a displays the superimposition of PL spectra of ITO/ZnO/P3HT and ITO/ZnO/P3HT:PCBM with ITO/P3HT and ITO/P3HT:PCBM respectively recorded at different excitation wavelengths.

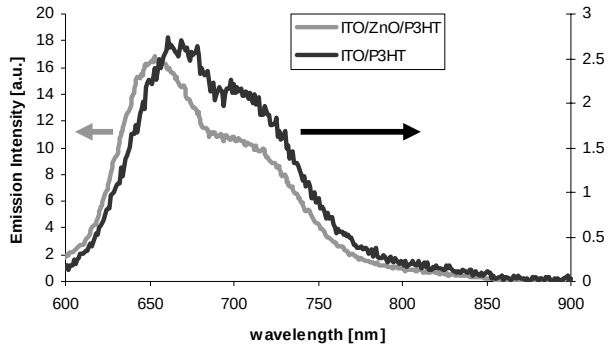

a

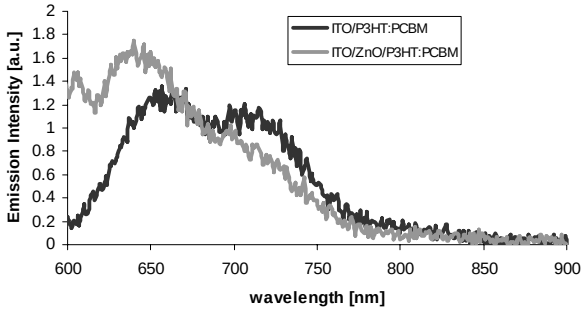

b

Fig. 6 – (a) *PL spectra of ITO/ZnO/P3HT and ITO/P3HT recorded at 530 nm excitation wavelength.* (b) *PL spectra of ITO/P3HT:PCBM and ITO/ZnO/P3HT:PCBM recorded at 510 nm excitation wavelength.*

Fig. 6a displays ITO/ZnO/P3HT and ITO/P3HT fluorescence spectra recorded by exciting at 530 nm. Despite the difference in emission intensity, both the junctions present an emission peak and a shoulder at long wavelengths which can be associated with the emission inside the polymer.

Fig. 6b shows ITO/P3HT:PCBM and ITO/ZnO/P3HT:PCBM fluorescence responses at 510 nm. ITO/P3HT:PCBM displays two peaks at 650 nm and 720 nm respectively that can be attributed to emission phenomena inside the blend. The peak at 720 nm is absent in the case of ITO/ZnO/P3HT:PCBM junction suggesting a better charge transfer in devices with that configuration.

Fig. 7 shows the quenching percentage estimated by comparing PL spectra - at 510 nm - of ITO/ZnO/P3HT and ITO/ZnO/P3HT:PCBM with respect to ITO/ZnO/P3HT. A quenching percentage of 92% is obtained in the case of ITO/ZnO/P3HT:PCBM device in a wide wavelength range, from 640 to 840 nm. This result underlines a very efficient photo-induced charge transfer across different layers of the ITO/ZnO/P3HT:PCBM solar cell based on electrodeposited ZnO.

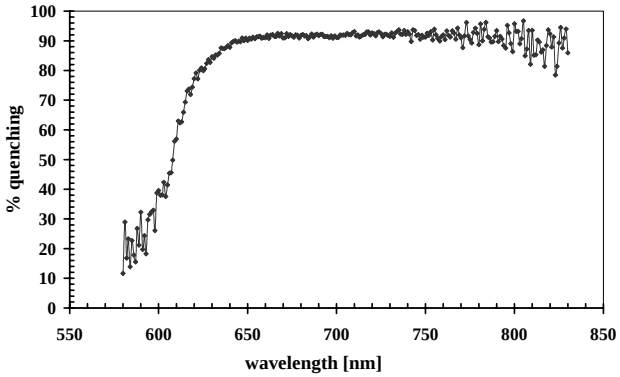

Fig. 7. Quenching percentage in ITO/ZnO/P3HT:PCBM with respect to ITO/ZnO/P3HT at 510 nm excitation wavelength.

4. Conclusions

A study about fluorescence phenomena occurring in hybrid solar cells based on electrodeposited ZnO has been performed. We have investigated ITO/ZnO/P3HT and ITO/ZnO/P3HT:PCBM taking ITO/P3HT and ITO/P3HT:PCBM as references. As expected, devices made of ITO/P3HT:PCBM blend have displayed a higher exciton quenching than devices made of P3HT. Quenching percentages have been calculated for both organic and hybrid devices. Quenching percentage in organic ITO/P3HT:PCBM has been calculated as the difference between ITO/P3HT and ITO/P3HT:PCBM fluorescence intensities divided by ITO/P3HT fluorescence intensity and its maximum value has been 60% at 1.82 eV emission. Quenching percentage in hybrid ITO/ZnO/P3HT:PCBM has been calculated with respect to ITO/ZnO/P3HT and its value has been 92% in a wavelength range from 640 to 840 nm.

In conclusion, the hybrid configuration ITO/ZnO/P3HT:PCBM displays a higher quenching percentage in a wider wavelength range than ITO/P3HT:PCBM, indicating a better photo-induced charge separation in e-ZnO based hybrid devices.

Acknowledgments

Dr. Viviana Figà would like to thank Dr. G. Ferrara from the University of Palermo, Dr. Y. Didane and Dr. J. Mawyin from Centre Interdisciplinaire de Nanoscience de Marseille for their helpful suggestions.

References

[1] Elif Arici, N. Serdar Sariciftci, Dieter Meissner, Encyclopedia of nanoscience and Nanotechnology, Vol.3, 929-944, Ed. H. S. Nalwa 2004.

[2] R.D. McCullough, P.C. Ewbank in: T.A. Skotheim (Ed.), Handbook of Conducting Polymers, Marcel Dekker, New York, 1998 (Chapter 9).
[3] H. Sirringhaus, N. Tessler, R. H. Friend, Science **280,** 1741 (1998).
[4] N. Camaioni, G. Ridolfi, G. C. Miceli, G. Possamai, M. Maggini, Adv. Mater. **14,** 1735 (2002).
[5] F. Padinger, R. S. Rittberger, N. S. Sariciftci, Adv. Funct. Mater. **13,** 85 (2003).
[6] I. Riedel, V. Dyakonov, Phys. Stat. Sol. (a) **201,** 1332 (2004).
[7] J. Mawyin, I. Shupyk, M. Wang, G. Poize, P. Atienzar, T. Ishwara, J. R. Durrant, J. Nelson, D. Kanehira, N. Yoshimoto, C. Martini, E. Shilowa, P. Secondo, H. Brisset, F. Fages, J. Ackermann, J. Phys. Chem. C **115,** 10881 (2011).
[8] R. Perez-Casero, A. Gutierrez-Llorente, O. Pons-y-Moll, W. Seiler, R. M. Defourneau, D. Defourneau, E. Millon, J. Perriere, P. Goldner, B. Viana, J. Appl. Phys. **97,** 054905 (2005)
[9] D. K. Hwang, S. H. Kang, J. H. Lim, E. J. Yang, J. Y. Oh, J. H. Yang, S. J. Park, Appl. Phys. Lett. **86,** 222101 (2005)
[10] Z. B. Shao, C. Y. Wang, S. D. Geng, X. D. Sun, S. J. Geng, J. Mater. Process. Technol. **178,** 247 (2006)
[11] Y. I. Alivov, J. E. Van Nostrand, D. C. Look, Appl. Phys. Lett. **83,** 2943 (2003)
[12] D. C. Oh, T. Suzuki, J. J. Kim, H. Makino, T. Hanada, M. W. Cho, T. Yao, Appl. Phys. Lett. **86,** 032909 (2005)
[13] W. Z. Xu, Z. z. Ye, Y. J. Zeng, L. P. Zhu, B. H. Zhao, L. Jiang, J. G. Lu, H. P. He, S. B. Zhang, Appl. Phys. Lett. **88,** 173506 (2006)
[14] A. Kuroyanagi, Jpn. J. Appl. Phys. **28,** 219 (1989)
[15] J. De Merchant, M. Cocivera, Chem. Mater. **7,** 1742 (1995)
[16] H. Khallaf, G. Chai, O. Lupan, L. Chow, S. Park, A. Schulte, J. Phys. D: Appl. Phys. **42,** 135304 (2009)
[17] T. Pauporté, D. Lincot, Appl. Phys. Lett. **75,** 3817 (1999)
[18] T. Pauporté, I. Jirka, Electrochimica Acta **54**, 7558 (2009).
[19] Y. Hames, Z. Alpaslan, A. Kosemen, S. Eren San, Y. Yerli, Sol. Energy **84,** 426 (2010).
[20] M. Wang, X. Wang, Sol. Energy Mater. Sol. Cells **92,** 766 (2008).
[21] M. Izaki, T. Omi, J. Electrochem. Soc. **143,** L53 (1996).
[22] H. Y. Fan, Phys. Rev. **82,** 900 (1951).
[23] R.E. Marotti, D.N. Guerra, C. Bello, G. Machado, E.A. Dalchiele, Solar Energy Materials and Solar Cells **82,** 85 (2004).
[24] R. N. Bhargava (Ed.), Properties of wide band gap II-VI semiconductors, EMIS Data reviewers Series No. 17, INSPEC, London, United Kingdom 1997.
[25] F. C. Krebs, Solar Energy Materials & Solar Cells **93,** 394 (2009).
[26] P. Vanlaeke, A. Swinnen, I. Haeldermans, G. Vanhoyland, T. Aernouts, D. Cheyns, C. Deibel, J. D'Haen, P. Heremans, J. Poortmans, J.V. Manca, Solar Energy Materials & Solar Cells, **90,** 2150 (2006).
[27] Erin L. Ratcliff, Judith L. Jenkins, Ken Nebesny, Neal R. Armstrong, Chem. Mater. **20,** 5796 (2008).
[28] V. Shrotriya, J. Ouyang, R.J. Tseng, G. Li, Y. Yang, Chem. Phys. Lett. **411,** 138 (2005).
[29] O. Lupan, T. Pauporté, L. Chow, B. Viana, F. Pellé, L. K. Ono, B. Roldan Cuenya, H. Heinrich, Appl. Surf. Sc. **256** 1895 (2010).
[30] T. Pauporté, I. Jirka, Electrochim. Acta, **54,** 7558 (2009).

*Corresponding author: viviana_fg@yahoo.it